Catalysis Science & Technology

ROYAL SOCIETY OF CHEMISTRY

PAPER

Cite this: *Catal. Sci. Technol.*, 2020, **10**, 3290

Photocatalytic asymmetric epoxidation of *trans*-stilbene with manganese–porphyrin/graphene-oxide nanocomposite and molecular oxygen: axial ligand effect†

Elahe Ahadi,[a] Hassan Hosseini-Monfared, *[ab] Alex Spieß[c] and Christoph Janiak [c]

Received 5th March 2020,
Accepted 25th April 2020

DOI: 10.1039/d0cy00441c

rsc.li/catalysis

An efficient, visible light-driven manganese–porphyrin photocatalyst was developed for the asymmetric epoxidation by molecular oxygen under mild conditions. A Mn–porphyrin complex covalently bonded to graphene oxide (GO) sheets was synthesized and characterized, where chirality is induced by enantiopure L-tartrate (tart), acting either as a counter ion or axial ligand. The heterogeneous photocatalyst GO-[Mn(T2PyP)(tart)](tart) showed an excellent epoxide selectivity of 100% toward the enantioselective epoxidation of *trans*-stilbene (ee 100%) in the presence of imidazole under irradiation with a white LED light source. An imidazole molecule hydrogen bonded to the high-valent manganese–oxo intermediate and $(tartrate)^-$ counter ion seems to be responsible for substantially enhancing the enantioselectivity of the catalyst. Also, an imidazole molecule coordinated to the metal centre is probably involved in the increased catalytic activity. With immobilized manganese porphyrin as photocatalyst, significant improvements in rate and enantioselectivity were attained by simply adding imidazole as an axial ligand and a hydrogen bond donor in *trans*-stilbene epoxidation. At the end of the reaction, GO-[Mn(T2PyP)(tart)](tart) was readily separated by filtration and reused for subsequent runs without any loss of its activity and enantioselectivity, resulting in a total turnover number (TON) of 3000.

Introduction

Enantiomerically pure chiral epoxides are valuable intermediates in organic synthesis, especially in the synthesis of various pharmaceuticals such as antitumor, antihypertensive, antibiotic, antidepressant and anti-HIV drugs.[1,2] In addition, chiral epoxides are used for the synthesis of various desirable chiral products *via* stereospecific ring-opening reactions in the preparation of agrochemicals, flavors, fragrances, chiral polymers, ferroelectric liquid crystals and chiral catalysts.[3,4] Manganese complexes show the potential to catalyze the symmetric and asymmetric[5,6] epoxidation of olefins with high efficiency[7] using various oxygen donors including molecular oxygen, which is a clean and cheap oxidant. Immobilization of the soluble transition-metal complexes onto solid supports is a prerequisite for their application as industrial catalysts, in order to prevent irreversible catalyst deactivation, to reduce the separation and synthesis cost and the product contamination by the homogeneous complex.[8]

Photocatalytic processes are ideal oxygenation method that are used for synthesis,[9] oxidative degradation of damaging organic pollutants,[10] in photodynamic therapy (PDT)[11] and oxidation of organic compounds.[12] Silva *et al.* prepared hybrid photocatalysts by sensitization of graphitic carbon nitride with free-base porphyrins attached to g-C_3N_4 through non-covalent interactions,[13] which were evaluated for the generation of hydrogen (H_2) from water splitting. They found that porphyrins with carboxy-substituent groups at the *meta* position showed the highest degree of H_2 generation from water splitting under UV and visible-light irradiation after 6 h. Jiang *et al.* used a Mo-Schiff base complex immobilized on GO/g-C_3N_4 sheets as photocatalyst in the epoxidation of olefins under simulated sunlight irradiation.[14] GO and active metal centres enhance the electron transfer for catalytic performance. Li *et al.* investigated the photocatalytic hydrogen evolution activity using 5,15-diphenyl-10,20-di(4-pyridyl)porphyrin (DPyP) grafted on GO through metal ions as interfacial linkers by means of

[a] *Department of Chemistry, University of Zanjan, 45195-313, Zanjan, Iran*
[b] *Department of Chemistry, Amirkabir University of Technology, Tehran, Iran. E-mail: hahomonfared@gmail.com*
[c] *Institut für Anorganische Chemie und Strukturchemie, Heinrich-Heine-Universität Düsseldorf, 40204 Düsseldorf, Germany. E-mail: janiak@hhu.de*

† Electronic supplementary information (ESI) available: UV-vis, FTIR and NMR spectra, GC-chromatograms, TGA and SEM–EDX data UV-vis, FTIR and NMR spectra, GC-chromatograms, TGA and SEM–EDX data. See DOI: 10.1039/d0cy00441c

electrostatic and coordination interaction.[15] The efficient electron transfer between the metal ions and DPyP/GO improved the photocatalytic hydrogen evolution performance. Fe_3O_4 magnetic nanoparticles sensitized by a free-base porphyrin were applied for the degradation of the pollutant bisphenol A in aqueous solution through the generation of singlet oxygen.[16] Various aldehydes were oxidized to the corresponding carboxylic acids with porphyrin/O_2 and Zn-porphyrin/O_2 under visible light in CH_3CN.[17] Aerobic photooxidation of various types of alcohols to the corresponding carbonyl compounds was performed with tetraphenylporphyrin (H_2TPP), ClFeTPP and ZnTPP as sensitizers using visible light under solvent-free conditions.[18] Safari *et al.* employed free-base porphyrins and metalloporphyrins as sensitizers in the aerobic epoxidation of alkenes under visible light.[19] The free-base porphyrin H_2TPP was a better sensitizer than other metallated and non-metallated porphyrins under these reaction conditions. 5,10,15,20-Tetrakis(pentafluorophenyl)porphyrin (H_2TF5PP) was used as photosensitizer for producing singlet oxygen for the treatment of water contaminated with metoprolol.[20] The adduct of H_2TPP with 2,3-dichloro-5,6-dicyano-1,4-benzoquinone (DDQ), that is, $H_2TPP(DDQ)_2$ was used as photosensitizer for the aerobic photooxidation of olefins in acetonitrile under white LED light.[21] Free-base porphyrins and metalloporphyrin derivatives were used as a photosensitizer for the epoxidation of cyclooctene by molecular oxygen. The order of reactivity for metalloporphyrins decreased as Zn > Mn > Fe > Co for a given porphyrin ligand.[22]

While free-base porphyrins are useful sensitizers for the production of singlet oxygen,[23] metalloporphyrins are much more versatile photocatalysts due to their coordination ability, promoting a wider range of oxidation reactions.[24] Elemans *et al.* developed a self-assembled system composed of a Mn–porphyrin trimer for the photocatalytic epoxidation of stilbene using O_2 as oxidant.[25] Sun *et al.* investigated the photocatalytic enantioselective epoxidation of terminal olefins with a non-heme chiral manganese catalyst, $[(R,R\text{-BQCN})Mn^{II}]^{2+}$; the enantiomeric excess was up to 60%. The authors used H_2O as oxygen source, $[Ru^{II}(bpy)_3]^{2+}$ as photocatalyst, and $[Co^{III}(NH_3)_5Cl]^{2+}$ as weak one-electron oxidant.[26] This was the first example for the use of a synthetic chiral Mn(IV)–oxo complex in the asymmetric epoxidation of olefins.

We herein report the photocatalytic epoxidation of *trans*-stilbene by a Mn–porphyrin immobilized on graphene oxide (GO) carrying enantiopure L-tartrate (tart) as counter ion and describe a remarkable axial ligand effect for substantially enhancing the enantioselectivity. GO possesses excellent characteristics such as large specific surface area, high electric and thermal conductivity.[27]

Results and discussion

Synthesis

The chemical structures and synthesis procedures of [Mn(T2PyP)(OAc)] and GO-[Mn(T2PyP)(tart)](tart) are

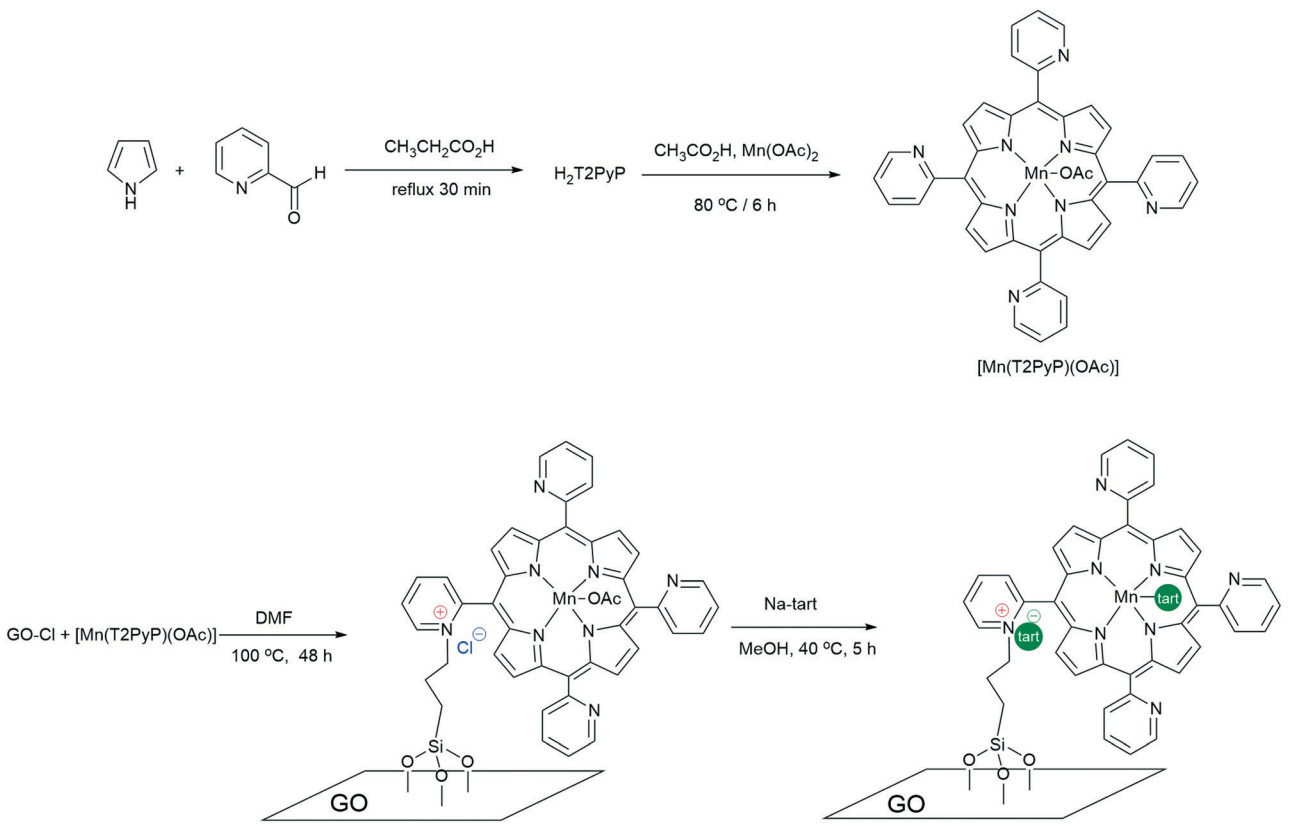

Scheme 1 Synthesis of chiral GO-[Mn(T2PyP)(tart)](tart).

illustrated in Scheme 1. First, the manganese complex of *meso*-tetra(2-pyridyl)porphyrin was prepared *via* the reaction of the synthesized H_2T2PyP and $Mn(OAc)_2$ in glacial acetic acid at 80 °C accompanied by *in situ* chemical oxidation of Mn(II) to Mn(III) with air.[28] The synthesized [Mn(T2PyP)(OAc)] was covalently bound to graphene oxide, which had been functionalized with propylchloride (GO–Cl), through the quaternization of one of the pyridine units. Just like the free H_2T2PyP molecule, also Mn-tetrapyridylporphyrin undergoes the quaternization reaction,[29] resulting in cationic species. The chlorinated GO surface is used in place of an alkyl halide. The reaction was carried out in DMF because polar solvents are known to increase the quaternization reaction rate which is otherwise slow due to steric factors.[30] Finally, the replacement of the axial ligand OAc^- and counter ion Cl^- was achieved by addition of excess sodium tartrate (Na-tart).

Photocatalyst characterization

IR spectroscopy. The presence of [Mn(T2PyP)OAc] on the GO surface was confirmed by FTIR measurements. The FTIR spectra of GO–Cl, [Mn(T2PyP)(OAc)], GO-[Mn(T2PyP)(OAc)]Cl, GO-[Mn(T2PyP)(tart)](tart) and Na-tart are collected in Fig. 1. As shown in Fig. S4 in the ESI,† GO exhibits fingerprint groups such as carboxylic species (1735 cm^{-1}), C=C stretching vibrations in aromatic rings (1630 cm^{-1}), OH deformation (1420 cm^{-1}), C–OH stretching (1228 cm^{-1}) and epoxy group C–O–C stretching (1059 cm^{-1}).[31] A peak at 700 cm^{-1} for ν(C–Cl) appeared after the functionalization of GO with 3-chloropropyl. Vibrational signatures at 1114 and 1036 cm^{-1} in GO–Cl, GO-[Mn(T2PyP)(OAc)]Cl and GO-[Mn(T2PyP)-(tart)](tart) (Fig. 1) are attributed to C–O and Si–O bonds, respectively.[32]

Absence of the ν(C–Cl) band in addition to the disappearance of ν(C=O) and ν(C–OH) bands of GO–Cl in the spectrum of GO-[Mn(T2PyP)(OAc)]Cl, Fig. 1(c), suggest that the quaternization step was successfully achieved in order to introduce the [Mn(T2PyP)(OAc)] groups on the surface of GO–Cl. A very broad band between 3140 and 3427 cm^{-1} in the spectrum of GO-[Mn(T2PyP)(tart)](tart) was assigned to the presence of the ν(O–H) of the hydroxyl groups (C–OH) and also to adsorbed water molecules on the GO (Fig. 1(d)). Comparing the spectrum of GO-[Mn(T2PyP)(tart)](tart) with that of GO-[Mn(T2PyP)(OAc)]Cl (Fig. 1(c)), there are new bands that appeared at 1714, 1118, and 1060 cm^{-1}, which correspond to the carbonyl and C–OH stretching vibrations as a result of the incorporation of the tartrate anion.

UV-vis spectroscopy. UV-vis absorption spectra of H_2T2PyP, [Mn(T2PyP)(OAc)] and GO-[Mn(T2PyP)(tart)](tart) are shown in Fig. 2. Comparison of the UV-vis spectra of H_2T2PyP and [Mn(T2PyP)(OAc)] confirmed the formation of the Mn-complex (Fig. 2);[33] the Soret band of H_2T2PyP was shifted from 419 nm to 464 nm and three of the four Q bands disappeared with the formation of [Mn(T2PyP)(OAc)]. For recording the UV-vis spectrum of the supported catalyst, a clean quartz cell surface was painted with the solid-aqueous suspension. The water was then evaporated, leaving a thin uniform layer of GO-[Mn(T2PyP)(tart)](tart) on the cuvette surface. The spectrum was recorded against a reference of water. The anchoring of Mn(T2PyP) on GO as GO-[Mn(T2PyP)(tart)](tart) leads to a blue shift in the Soret band compared to [Mn(T2PyP)(OAc)]. The Soret peak shifted to 433 nm and appeared as a broad absorption peak which confirms the immobilization of the Mn(T2PyP) complex. Additionally, the composite shows a strong absorption band at 304 nm (the $\pi \rightarrow \pi^*$ transition of graphitic C=C bonds), which corresponds to that of graphene oxide with a red-shift of 76 nm.[34] These results indicate that in the ground state attachment of the Mn(T2PyP) moiety on GO has perturbed both the electronic state of the graphene oxide and of Mn(T2PyP).

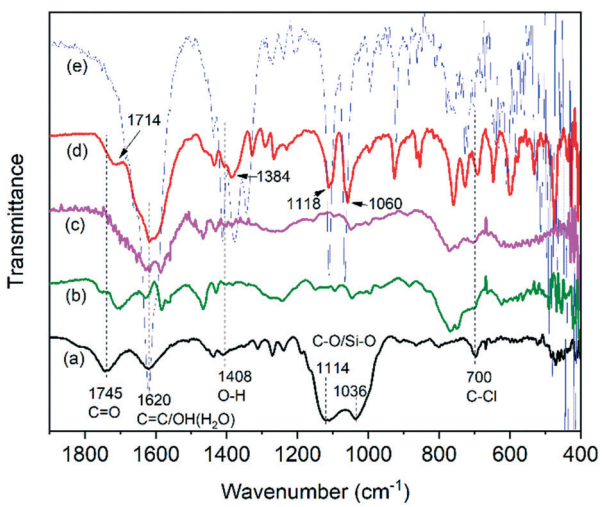

Fig. 1 FTIR spectra of (a) GO–Cl, (b) [Mn(T2PyP)(OAc)], (c) GO-[Mn(T2PyP)(OAc)]Cl, (d) GO-[Mn(T2PyP)(tart)](tart) and (e) Na-tart.

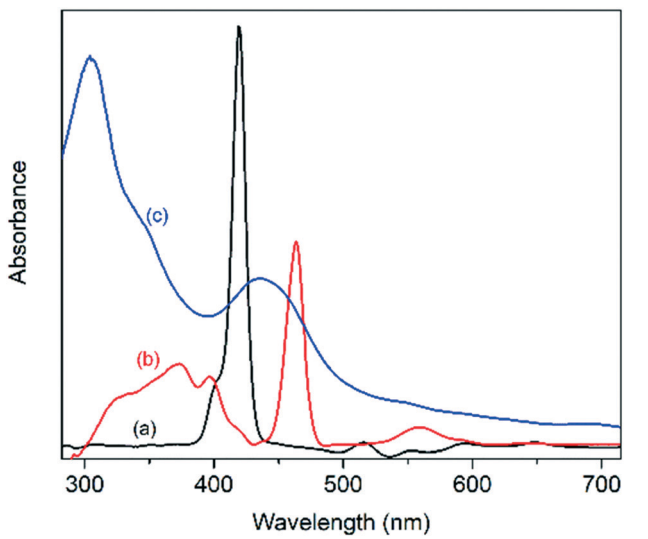

Fig. 2 UV-vis absorption spectra of (a) H_2T2PyP (Soret band at 419 nm in CH_2Cl_2), (b) [Mn(T2PyP)(OAc)] (Soret band at 464 nm in CH_2Cl_2) and (c) a film of GO-[Mn(T2PyP)(tart)](tart) with peaks at 304, 343 (shoulder) 433 and 691 nm.

Photoluminescence. Porphyrins are considered to be most interesting compounds from the aspect of photophysical properties, owing to their rigidity and aromatic electronic system. The fluorescence emission spectra of [Mn(T2PyP)-(OAc)] and GO-[Mn(T2PyP)(tart)](tart) (Fig. 3) exhibit two distinct maxima, a strong fluorescence band near 450 nm, and an emission band of smaller intensity around 350 nm upon excitation at 280 nm. The relatively weak Soret bands which appear in the 380–440 nm regions are assigned to the S2/S0 transitions. The strong Q bands are assigned to the S1/S0 transitions. Using higher concentrations of [Mn(T2PyP)-(OAc)] led to fluorescence with lower intensities. This finding suggests easy aggregation of homogeneous [Mn(T2PyP)(OAc)] in water;[35] the monomeric form shows fluorescent emission with higher intensity. Aggregation lowers the photoactivity of molecules through dissipation of energy by aggregate formation.[36] Aggregates take up electronic energy and convert it into vibrational motion. The amount of Mn(T2PyP) is lower in the composite than in the pure form. So the composite GO-[Mn(T2PyP)(tart)](tart) exhibits 14% quenching of the fluorescence emission.

Thermogravimetric analysis. The thermal decomposition behavior of GO, GO–Cl, GO-[Mn(T2PyP)(tart)](tart) and [Mn(T2PyP)(OAc)] was investigated by thermogravimetric analysis (TGA) under N_2 atmosphere (Fig. 4). Several weight loss steps were observed in the TGA curve for the GO nanosheets. The weight loss at 30–100 °C (about 14%) is primarily due to the loss of H_2O molecules that are physically adsorbed on the surface of the GO nanosheets. The weight loss observed at 100–200 °C (about 37%) and 200–280 °C (about 13%) are due to the thermal decomposition of stable hydroxyl, epoxide and carboxylic groups on the basal plane of GO nanosheets. The final step at 280–700 °C (about 12%) is mainly due to the combustion of the carbon skeleton of GO nanosheets.[37] On the other hand, the weight loss for GO–Cl

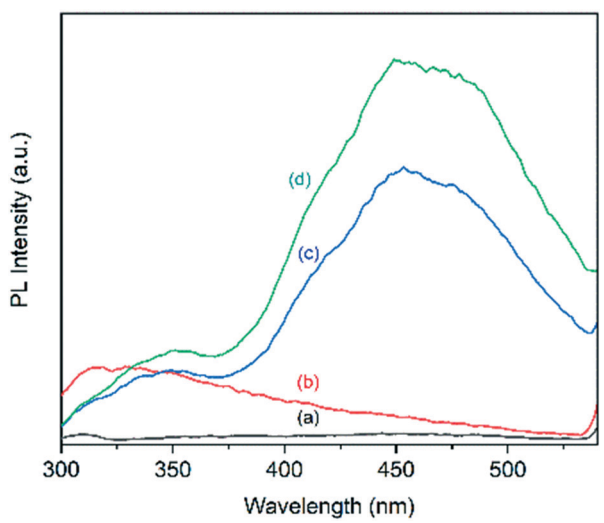

Fig. 3 Fluorescence spectra (upon excitation at λ = 280 nm) of (a) GO, (b) GO–Cl, (c) GO-[Mn(T2PyP)(tart)](tart) and (d) [Mn(T2PyP)(OAc)]; the samples were dispersed/dissolved in 3 mL of water.

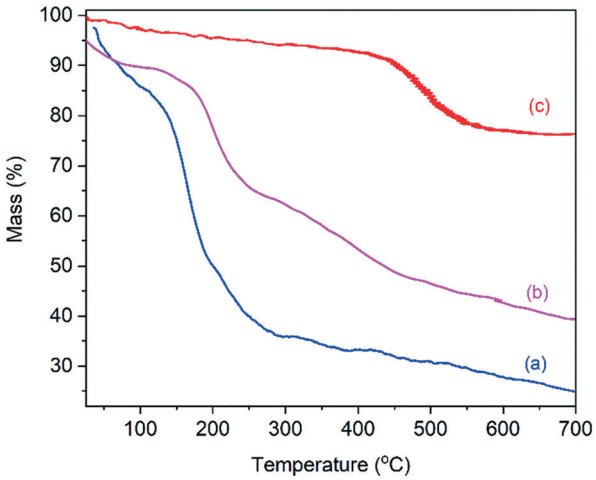

Fig. 4 Thermogravimetric analysis of (a) GO, (b) GO–Cl and (c) GO-[Mn(T2PyP)(tart)](tart) at a heating rate of 10 °C min^{-1} under nitrogen atmosphere.

at 30–100 °C is due to the desorption of physically adsorbed water which is about 10%. The weight loss at 100–260 °C and 260–465 °C (about 25% and 17%, respectively) can be attributed to the loss of the products formed during the condensation reaction of the silanes on the surface of the GO–Cl nanosheets. The weight loss at 470–700 °C (about 9%) is due to thermal oxidative decomposition of the grafted silanes.[38] Results show that the total residual masses at 700 °C for the GO and GO–Cl powders are about 25% and 40%, respectively, representing a significant thermal stability improvement of GO–Cl through functionalization of GO by (3-chloropropyl)triethoxysilane.

GO-[Mn(T2PyP)(tart)](tart) shows 7% weight loss in the range of 25–400 °C, evidently owing to evaporation of water molecules, which are trapped in the material. Then, another major mass loss (17%) occurs in the range of 400–700 °C owing to decomposition of the porphyrin (Fig. 4(c)). The composite GO-[Mn(T2PyP)(tart)](tart), showed the highest stability and the remaining mass at 700 °C is 76%. Porphyrins have been used in the catalysis field because of their special structure and high thermal stability.[39]

SEM and TEM analysis. Micro-structural features and the morphology of the GO-[Mn(T2PyP)(tart)](tart) material were analyzed by SEM and TEM (Fig. 5). The SEM images in Fig. 5 reveal that the GO consists of randomly aggregated, crumpled sheets closely associated with each other and forming a disordered solid. Fig. 5 also shows twisted sheets for GO-[Mn(T2PyP)(OAc)]Cl and GO-[Mn(T2PyP)(tart)](tart). The transmission electron microscopic image in Fig. 5 reveals the nanoscopic features with the known crumpled structure of GO and has the grafted Mn–porphyrin indicated by white arrows.

The elemental composition of GO, GO-[Mn(T2PyP)(OAc)]Cl and GO-[Mn(T2PyP)(tart)](tart) was analyzed by EDX (see Fig. S7 in ESI†). GO is found to be mainly composed of carbon and oxygen along with traces of sulphur. The loading of the

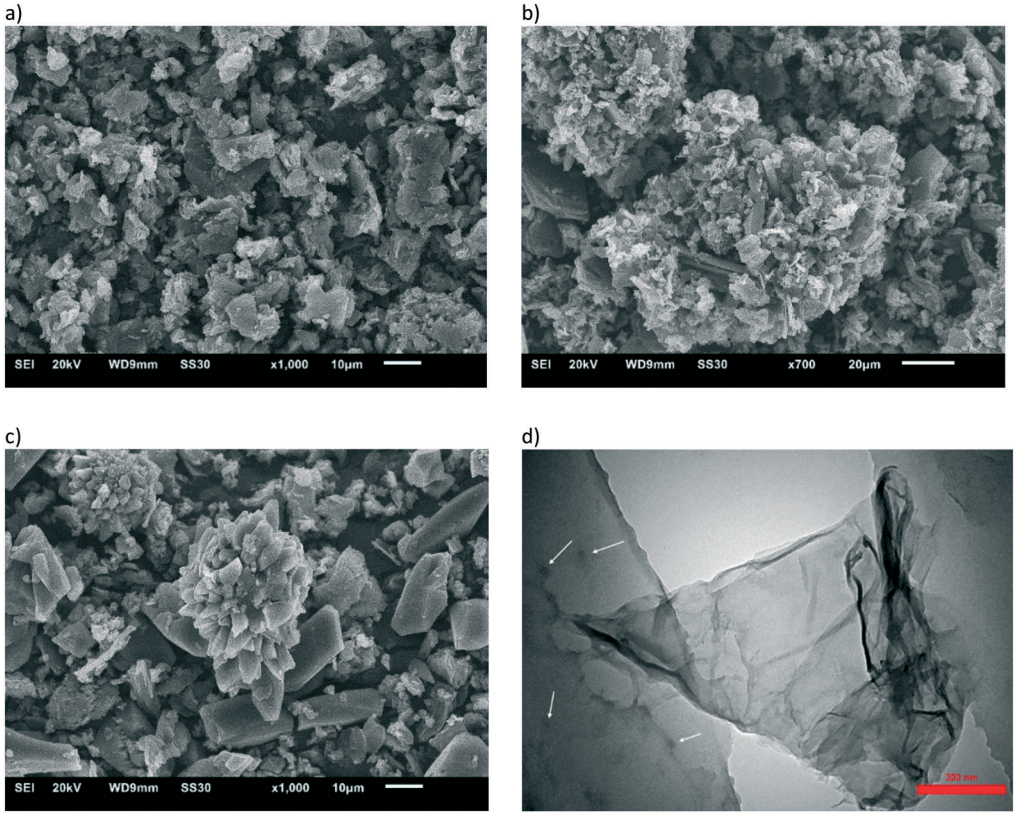

Fig. 5 SEM micrographs of (a) GO, (b) GO-[Mn(T2PyP)(OAc)]Cl and (c) GO-[Mn(T2PyP)(tart)](tart) and (d) TEM of GO-[Mn(T2PyP)(tart)](tart) (scale bar 300 nm). The white arrows in the TEM image indicate the Mn–porphyrin.

[Mn(T2PyP)(OAc)] complex on GO introduces manganese, chlorine and silicon, which are detected by EDX. From EDX analysis the Mn content in GO-[Mn(T2PyP)(OAc)]Cl is ~0.23 wt% (after deducting for the Au, Cu and Zn content). In the EDX analysis of GO-[Mn(T2PyP)(tart)](tart) the Mn content of ~0.09 wt% is in very good agreement with the value of ~0.1 wt% found by AAS. Atomic absorption measurement showed 18 μmol manganese per gram of GO-[Mn(T2PyP)(tart)](tart), corresponding to 0.098 wt% Mn. From the molar Mn : Cl ratio of 0.06(1) : 2.9(1) in GO-[Mn(T2PyP)(OAc)]Cl and of 0.02(1) : 0.74(3) in GO-[Mn(T2PyP)(tart)](tart) it is evident that only a small fraction of the chloropropylsilanol functions has been utilized for quaternarization and complex binding. At the same time the molar Si : Cl ratio of 2.5(1) : 2.9(1) and 0.50(3) : 0.74(3) is not far from the expected unity. The reduced oxygen percentage in GO-[Mn(T2PyP)(OAc)]Cl from 18(2) wt% to 7(1) wt% (still including the Au, Cu, Zn content) is attributed to the partial deoxygenation in GO during the Mn–porphyrin grafting, which is confirmed by TGA. The EDX analysis for GO-[Mn(T2PyP)(tart)](tart) then shows an increased oxygen content again (up to 21(2)) wt% which is in accordance with the replacements of acetate and chloride anions with tartrate anions as well as the deposition of Na-tart, the latter being evidenced by the high sodium content of 11(1) wt%.

Photocatalysis. The chiral GO-[Mn(T2PyP)(tart)](tart) was characterized using UV-vis, PL, SEM, EDX and TEM techniques. The spectroscopic data are in good agreement with the proposed composition of the chiral Mn–porphyrin. Epoxidation of *trans*-stilbene was used as a test reaction for homogeneous [Mn(T2PyP)(OAc)] and heterogeneous chiral GO-[Mn(T2PyP)(tart)](tart) as catalyst precursors with molecular oxygen as an oxidizing agent under white LED light. Isobutyraldehyde (IBA), which has been proven to be the best co-reductant reagent, was used in combination with dioxygen. IBA is one of the most economical and efficient reagents to promote the generation of acylperoxy radicals, recognized as epoxidation intermediates.[40] Imidazole was used as an axial ligand. The molar ratios of the catalyst and reactants were 1 : 2 : 1000 : 5000 for [Mn(T2PyP)(OAc)] : imidazole : *trans*-stilbene : isobutyraldehyde. The results from the catalytic epoxidation of *trans*-stilbene by [Mn(T2PyP)(OAc)] are summarized in Table 1. Photocatalytic oxidation produced *trans*-stilbene epoxide and isobutyric acid due to co-oxidation of the oxygen acceptor isobutyraldehyde as indicated by TLC, GC, ^{1}H-NMR and ^{13}C-NMR analyses (Fig. S8–S11† and Table 1, entries 1 and 2).

The absence of the starting substrate peak at 7.13 ppm as well as the appearance of a peak at 3.85 ppm in the ^{1}H-NMR and at 62.75 ppm in the ^{13}C-NMR spectra, corresponding to the epoxide functional group, confirmed the conversion of *trans*-stilbene to the epoxide. While the whole conversion was complete in 30 min using the imidazole-containing or complete photocatalytic system, in the absence of imidazole the reaction rate decreased to half (Table 1, entries 1 and 2).

Table 1 Photocatalytic oxidation of *trans*-stilbene under an O_2 atmosphere in the presence of [Mn(T2PyP)(OAc)][a]

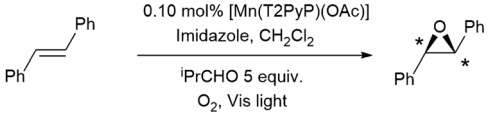

Entry	Conditions	Conversion (%)	Time
1	Complete system[a]	100	30 min
2	No imidazole	100	60 min
3	Dark	No reaction	80 min
4	No ^{i}PrCHO	No reaction	24 h
5	No catalyst	No reaction	24 h

[a] Catalyst [Mn(T2PyP)(OAc)] (0.50 mg, 0.71 μmol), imidazole (1.42 μmol), *trans*-stilbene (0.71 mmol), ^{i}PrCHO (3.55 mmol), oxygen 1 bar, CH_2Cl_2 1 mL at room temperature under LED (40 W) light.

Similar to our finding it has been reported that Fe- and Mn–porphyrins alone are unable to catalyze olefin epoxidation by H_2O_2 in the absence of an axial ligand.[41] From a study of various Mn–porphyrin catalysts and nitrogen-base co-catalysts, Mn(TDCPP)Cl in the presence of 10–20 equiv. of imidazole was the most efficient system (H_2TDCPP = *meso*-tetrakis(2,6-dichlorophenyl)porphyrin). With a highly restricted Mn–porphyrin as catalyst, the utilization of organic bases as axial ligand can lead to a dramatic increase in regioselectivity for alkene epoxidation.[42] The presence of an axial ligand improves the reaction rates and the stereoselectivity of the reaction[43] by facilitating the formation and stabilization of the proposed formally Mn^{IV}═O intermediate. It was also shown that the axial ligand coordination enhances the activity of oxomanganese(v) 5,10,15-tris(pentafluorophenyl)corrole, Mn^{V}O(tpfc), towards styrene. The turnover frequency (TOF) was increased about 7 times in the presence of imidazole (catalyst/ligand, 1 : 10) by lowering the binding energy of the Mn═O bond in (tpfc) Mn^{V}O.[44] Axial ligation exerts a profound effect on the structure and activity of [Mn(T2PyP)(OAc)] similar to reported metalloporphyrins.[45] The elongation of the Mn–O bond distance and destabilization of the high-valent manganese(v)–oxo intermediate could occur due to the coordination of imidazole at the position *trans* to the manganese–oxo bond which increases the rate of reduction of the manganese–oxo porphyrin.[46]

Control experiments showed that no reaction occurs in the absence of light, IBA or catalyst [Mn(T2PyP)(OAc)] (Table 1, entries 3–5). Furthermore, no enantiomeric excess (ee) was observed.

Photocatalytic activity of chiral GO-[Mn(T2PyP)(tart)](tart). The composite GO-[Mn(T2PyP)(tart)](tart) with the asymmetric tart anions showed highly remarkable activity and enantioselectivity (ee 100%) in the photocatalytic oxidation of *trans*-stilbene by molecular oxygen in the presence of imidazole and white light (Table 2, entry 1). Investigation of the reaction by ^{1}H-NMR and ^{13}C-NMR after separation of the catalyst, confirmed the formation of *trans*-stilbene epoxide as the sole product (Fig. S8 and S9 in ESI†). Possible reaction products such as benzaldehyde or benzoic acid from breaking the stilbene double bond are not formed. Isobutyric acid was produced due to co-oxidation of the oxygen acceptor isobutyraldehyde. *Trans*-Stilbene is quantitatively converted to stilbene epoxide after 80 min. The use of light and imidazole leads to extremely important improvements in the catalytic activity of Mn(T2PyP); this is clearly seen in comparison with the activities of the similar Mn–porphyrin catalysts. The activity and/or enantioselectivity of this system is much better than [Mn(T4PyP)(OAc)]Cl immobilized on

Table 2 Photocatalytic oxidation of *trans*-stilbene by chiral GO-[Mn(T2PyP)(tart)](tart)[a]

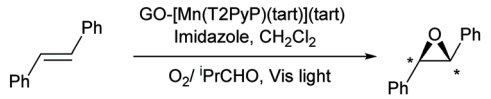

Entry	Conditions	Results	Time
1	Complete system[a]	Conversion 100% ee 100% (*R*,*R*)-epoxide	80 min
2	No imidazole	Conversion 100% ee 6.25% (*R*,*R*)-epoxide	140 min
3	Dark	No reaction	8 h
4	No ^{i}PrCHO	No reaction	24 h
5	No catalyst	No reaction	24 h
6	No O_2	No reaction	24 h

[a] Reaction conditions: catalyst chiral GO-[Mn(T2PyP)(tart)](tart) (0.0397 g, containing 0.71 μmol Mn), imidazole (1.42 μmol), *trans*-stilbene (0.71 mmol), isobutyraldehyde (3.55 mmol), oxygen 1 bar, CH_2Cl_2 1 mL at room temperature under LED (40 W) light. TON = 1000; turnover number (TON) = the average number of chemical conversions of substrate molecule that a single catalytic site executes.

chiral GO (reaction time 6 h at 52 °C, 100% ee),[47] Fe_3O_4-[Mn(TCPP-Ind)Cl] (8 h, 76% ee),[6] GO-[Mn(T4PyP)(tart)] (10 min, 58% ee),[48] SBA15-[Mn(T4PP)(tart)] (4 h at 45 °C, 66% ee)[49] and SBA15-[Mn(TCP-R)Cl] (8 h, 74% ee)[50] in the oxidation of *trans*-stilbene by molecular oxygen. The main differences between the present photocatalyst and the previously reported catalyst ([Mn(T4PyP)(OAc)] immobilized on chiral GO, GO*-[Mn(T4PyP)OAc])[47] are the use of 50 W white visible light and imidazole as axial ligand, using a higher molar ratio of olefin/RCHO (1 : 5 instead of 1 : 3), room temperature instead of 52 °C and very close proximity of the chiral tartrate counter ion to the catalyst active center (manganese and plausible high-valent Mn–oxo). The compound GO*-[Mn(T4PyP)OAc] did not show any photocatalytic activity for the epoxidation of olefins.

There are rare reports on the photocatalytic oxidation of *trans*-stilbene. Photooxidation of *trans*-stilbene by O_2 catalyzed with riboflavin tetraacetate (RFT: R = $C_{13}H_{19}O_8$) in H_2O/CH_3CN (irradiation of blue-emitting 440 nm–3 W LED as light source) led to benzaldehyde (69% yield) within 5 min, leaving only 2% of starting material and 2% of *cis*-stilbene.[51] Stacks of trimeric manganese porphyrins mediate the epoxidation of *cis*-stilbene with O_2/RCHO at room temperature within 30 min with complete conversion under irradiation with a 150 W xenon lamp in CH_2Cl_2.[25]

Control experiments (Table 2) proved the essential role of the axial ligand (imidazole), light, IBA, photocatalyst and O_2 as oxidant (Table 2, entries 2–6). Our preliminary experiments showed the molar ratio of 1 : 5 for *trans*-stilbene : IBA results in the highest rate and complete conversion. For example, the oxidation of *trans*-stilbene with a molar ratio of 1 : 2 *trans*-stilbene : IBA was less than 50% after 2 h. Probably, in order to have the appropriate concentration of the acyl radical (or acylperoxy radical) in the plausible equilibrium, a higher ratio of RCHO : olefin is needed (see the mechanism section below). Light proved to be crucial for the epoxidation to happen: no conversion of stilbene was observed in the dark at 40 °C; no reaction occurred after 80 min (Table 2, entry 3). It is clear that light enables the catalytic reaction.

Effects of solvents were screened by performing the photocatalytic oxidation of *trans*-stilbene by O_2/RCHO/GO-[Mn(T2PyP)(tart)](tart)/imidazole under visible light in DMF, DMSO, CCl_4, $CHCl_3$ and CH_2Cl_2 as solvent. The use of $CHCl_3$ as solvent led to a significant decrease in the conversion; only a trace amount of the epoxide was formed. And no product was observed in DMF, DMSO and CCl_4. The studies of solvent effects exclude the involvement of singlet oxygen ($^1O_2$) as reactive intermediate produced by Mn–porphyrin as photosensitizer. Lifetime of singlet oxygen is long in DMF and DMSO solvents, due to little absorption at 1267 nm (singlet oxygen absorption region).[36]

The reaction proceeded asymmetrically only in the presence of imidazole (Fig. S12† and Table 2, compare entries 1 and 2); enantiomeric excess (ee) was 6% in the absence of imidazole. In addition, the presence of imidazole increased the rate, and the required time for completion of the reaction decreased from 140 min to 80 min. Similar to our finding, it has been reported that axial ligation increases regioselectivity towards less substituted C–C double bonds in metalloporphyrin-catalyzed diene epoxidation.[42] To better understand the role of nitrogen bases in activating the Mn–porphyrin catalyst, the co-catalytic effects of three classes of nitrogen donors and the effect of the axial ligand : catalyst molar ratio were investigated (Table 3 and Fig. 6).

The rate of the oxidation in the presence of the strong π-donor imidazole (reaction time 80 min) was far better than 4-aminopyridine (100 min) and nicotinamide (135 min). Imidazole is a far better co-catalyst than pyridine class because of its stronger π-donor ability and hydrogen-bonding feature. Imidazole and pyridines were chosen since they are generally much better co-catalysts than pure σ-donors.[52]

The highest rate was obtained when the imidazole : catalyst ratio was 2 (Fig. 6). The co-catalytic effect is caused by the proximal and distal interactions of imidazole with the catalysts. Manganese–porphyrins normally form complexes with N-donor axial ligands, which coordinate in the position *trans* to Mn=O and increase the rate of oxygen atom transfer from the corresponding Mn(oxo)(porphyrin) to the substrate.[53] It is well known that thiolate of amino acid residues acts as the fifth ligand in cytochrome P450 enzymes[54] and many reports highlight the effect of axial ligation on the selectivity of metalloporphyrins in the reactions.[42,45,55,56]

The oxidation of styrene by GO-[Mn(T2PyP)(tart)](tart) was not successful. The conversion of α-methylstyrene to α-methylstyrene oxide was 6.5% under complete-catalyst conditions.

Mechanistic considerations. With regard to the experimental results, a possible mechanism is proposed as shown in Scheme 2 for the asymmetric epoxidation of *trans*-stilbene with molecular oxygene/isobutyraldehyde catalyzed by the chiral Mn–porphyrin under visible light. The proposed mechanism involves (i) the promotion of the [(porph)(Im)Mn(III)] complex to a photoexcited state,

Table 3 Axial ligand effect on the rate of the oxidation of *trans*-stilbene[a]

Axial ligand	Time (min)	Conversion (%)
	80	100
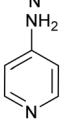	100	100
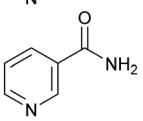	135	100

[a] Reaction conditions as in Table 1. Catalyst GO-[Mn(T2PyP)(tart)](tart) (0.71 μmol), axial ligand (1.42 μmol), *trans*-stilbene (0.71 mmol), ^{i}PrCHO (3.55 mmol), oxygen 1 bar, CH_2Cl_2 1 mL at room temperature under LED (40 W) light.

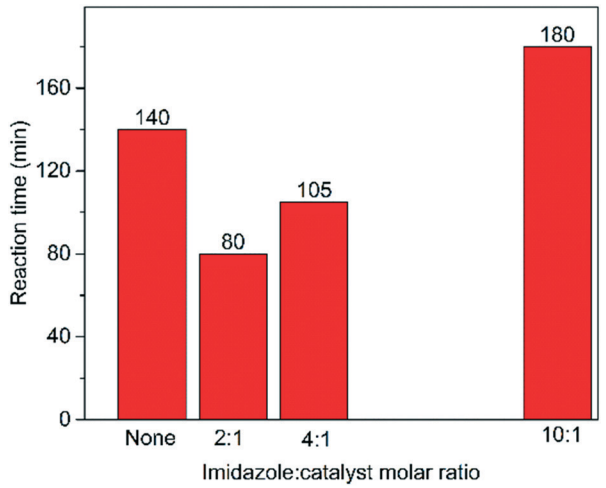

Fig. 6 Effect of imidazole : Mn–porphyrin molar ratio on the rate of the oxidation. Reaction conditions as in Table 1.

[(porph)(Im)Mn(III)]*, by absorbing white visible light in the first step. (ii) The [(porph)(Im)Mn(III)]* reacts with the aldehyde to generate the [Mn(II)] and an acyl radical which then reacts with molecular oxygen to produce an acylperoxy radical ($RCO_3^{\bullet}$).[57] The $RCO_3^{\bullet}$ can react with the olefin to yield the epoxide and an $RCO_2^{\bullet}$ radical which is finally converted to carboxylic acid (step iii).[58] However, obtaining the asymmetric *trans*-stilbene oxide suggests that direct oxidation of the olefin with the peracid, pathway (iii), is not followed under this condition. Another possibility for the acylperoxy radical is to follow pathway (iv) and to react with [(porph)(Im)Mn(II)] to generates an acylperoxo complex, [(porph)(Im)Mn(III)O_2COR]. This intermediate may also be produced by the addition of an acyl radical to a superoxide complex [(porph)(Im)Mn(IV)($O_2^{\bullet-}$)] obtained by the reaction of O_2 with [(porph)(Im)Mn(II)], step (v). In the following step (vi), the subsequent reductive O–O bond cleavage produces [(porph)(Im)Mn(IV)(O)] and isobutyric acid (RCO_2H). The subsequent asymmetric oxidation of the olefin by [(porph)(Im)Mn(IV)(O)] to yield the chiral olefin oxide with concomitant regeneration of [(porph)(Im)Mn(II)] happens in step (vii). A similar mechanism has been previously described in the literature using O_2 and an aldehyde.[59] Probably the same mechanism is followed for the homogeneous catalyst [Mn(T2PyP)(OAc)]. However, because of the ease of access of olefin to the active Mn–oxo center the oxidation rate is high.

Our experimental findings and conclusions are as follows: (a) No reaction occurs in dark even after 8 h (Table 2, entry 3). This finding indicates that the catalyst is activated by light, probably through a photoexcited state on the porphyrin that allows the activation of molecular oxygen at room temperature. Activation of oxygen happens by Mn–porphyrin acting as sensitizer due to its strong light absorption property. Metalloporphyrins are attractive compounds for applications in photochemical reactions, in particular oxidation reactions, because they absorb strongly in the visible spectrum.[60] The possibility that electronically excited, metastable singlet-oxygen molecules might be involved as reactive intermediate in Mn–porphyrin sensitized photooxygenation reactions was not supported by the studies of solvent effects. It has been reported that upon irradiation into the spectral region of the Soret band (433 nm) a coordinatively unsaturated and catalytically reactive manganese(II)–porphyrin is formed.[61] The excited manganese(II)–porphyrins generated photochemically react stepwise with O_2 with formation of the oxygen-transfer species [(porph)Mn^{IV}=O]. Manganese porphyrins have attracted special attention because of their high-valent oxo species are related to manganese oxo species in the oxygen-evolving center (OEC) of photosystem II. A similar mechanism (formation of a [Mn^{IV}-superoxo] complex) has been proposed for the photocatalytic oxidation of 10-methyl-9,10-dihydroacridine by O_2 with manganese(III) porphyrins[62] and catalytic oxygenation of olefins using (tetraarylporphyrinato)-manganese(III) complexes with O_2 and visible light with the intermediary of [Mn^{III}-superoxido].[63] Free radical mechanisms have been reported for the photocatalytic oxidation of

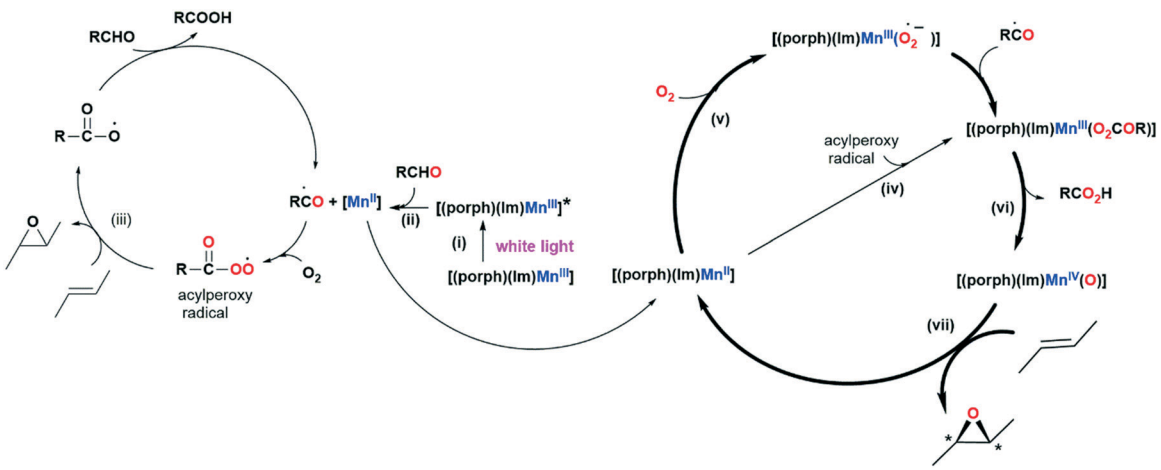

Scheme 2 Suggested mechanism for the visible-light-driven photocatalytic asymmetric epoxidation of *trans*-stilbene by GO–Mn(porphyrin)/O_2/RCHO/Im. Species charges are omitted for clarity.

stilbene by self-assembled Mn–porphyrin[25] and the oxidation of PPh_3 by Mn-corroles.[64] However, porphyrins and phthalocyanines, especially the zinc derivatives, can act as photosensitizers due to their intense absorption and trigger the formation of $^1O_2$.[17,65,66] High triplet-state quantum yields and long lifetimes are required for efficient sensitization and these criteria may be fulfilled by the incorporation of a diamagnetic metal such as zinc, aluminum or silicon into the porphyrin and phthalocyanine macrocycles; transition metal (such as Co, Cu and Fe) complexes of these compounds do not show photosensitizing activity.[36] Long lifetimes of the excited state enhance the number of diffusional encounters between the triplet excited state and ground state O_2.

(b) The reaction is initiated by isobutyraldehyde. The olefin epoxidation by O_2 in the presence of metal porphyrins and an aldehyde as an oxygen acceptor proceeds *via* a free radical mechanism.[67] In agreement with earlier studies, the epoxidation of *trans*-stilbene in DMSO under the standard conditions was fully quenched; therefore a singlet oxygen pathway is ruled out. The reaction of molecular oxygen with aldehyde can produce an acylperoxy species, which is an efficient oxidizing agent for olefin epoxidations.[68] Formation of isobutyric acid also confirms the involvement of perbutyric acid (RCO_3H) which is the product of the reaction of isobutyraldehyde with O_2/Mn(porph).

(c) The probable active oxidizing intermediate is the peracid of isobutyraldehyde ($^iPrCO_3H$) since the system does not work in the absence of ^{i}PrCHO, and isobutyric acid is the coproduct of the oxidation (Table 2, entry 4).

(d) Presence of an axial ligand (imidazole) significantly increases the rate and at the same time induces chirality in the product (Table 2, entries 1 and 2).[47] The reaction goes through the interaction between olefin and [(porph)(Im)-Mn=O] by considering manganese–oxo as the accepted intermediate in the oxygenation reactions catalysed by Mn–porphyrin.[69,70]

Asymmetric induction occurs mainly through the $(tartrate)^-$ counter ion not through axially coordinated tartrate. During the reaction the axially coordinated tartrate is replaced with imidazole. The imidazole ligand enhances the electron donation from Mn(III) to the peracid anion (Scheme 2) and facilitates the formation of the high valent Mn=O species. Furthermore, oxygen atom transfer from Mn^{IV}=O to the olefin is accelerated by the coordinated imidazole ligand. In addition, the presence of excess imidazole around the reaction centre, keeps the $(tartrate)^-$ counter ion as close as possible to the reactive intermediate center, Mn(IV), by hydrogen bonds, thereby enforcing chirality in the produced epoxide (Fig. 7).

The strong π-donor imidazole (Im) is a far better co-catalyst than other nitrogen donors. The coordinated imidazole can form hydrogen bonds with uncoordinated imidazole molecules through its N–H group which increases its donor ability.[52] Distal hydrogen bonding between the coordinated oxidant and one or more imidazoles is also

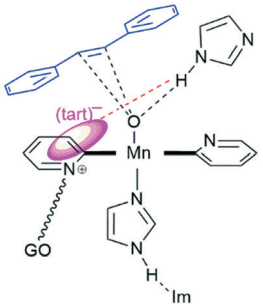

Fig. 7 Suggested intermediate [(T2PyP)(Im)-Mn^{IV}O].

plausible to facilitate (porphyrin)Mn–O formation.[52,71] The Mn–O unit is stabilized by intramolecular hydrogen-bonding networks surrounding the Mn–oxo unit in Mn-complexes.[72] There is also evidence that the addition of Lewis or Brønsted acids to the high-valent manganese–oxo complex [Mn^V(O)(TBP8Cz)] results in the stabilization of a valence tautomer [Mn^{IV}(O-LA)($TBP8Cz^{\bullet+}$)] and enhances the substrate C–H activation, (TBP8Cz = octakis(*p*-tertbutylphenyl) corrolazinato^{3-}).[73]

Stability of the photocatalyst. The photocatalyst GO-[Mn(T2PyP)(tart)](tart) could be recycled up to three times without any significant reduction in its catalytic activity or enantioselectivity (Fig. 8). In addition, after completion of the reaction, no detectable leaching of manganese was found by atomic absorption analysis. Analysis of the recovered catalyst, after having been used three times, by FTIR, SEM and DRS (Fig. 9) showed the intact Mn–porphyrin structure and morphology. The immobilization of Mn(T2PyP) onto GO, in addition to providing the possibility of having a chiral counter ion ($tart^-$), allows catalyst recovery and reuse, easy product recovery and higher turnover number, while minimizing the environmental impact. A total TON (turnover number, the molar ratio of stilbene oxide and the corresponding manganese catalyst) of 3000 was obtained.

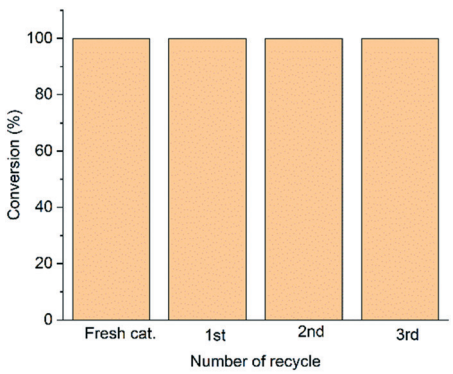

Fig. 8 Catalyst recyclability study for the oxidation of *trans*-stilbene. Reaction conditions: catalyst chiral GO-[Mn(T2PyP)(tart)](tart) (0.0397 g, containing 0.71 μmol Mn), imidazole (1.42 μmol), *trans*-stilbene (0.71 mmol), isobutyraldehyde (3.55 mmol), oxygen 1 bar, CH_2Cl_2 1 mL at room temperature under white LED (40 W) light for 80 min. Enantiomeric excess was more than 99% in each recycling experiment. Total TON (turnover number) for three recycle runs was 3000.

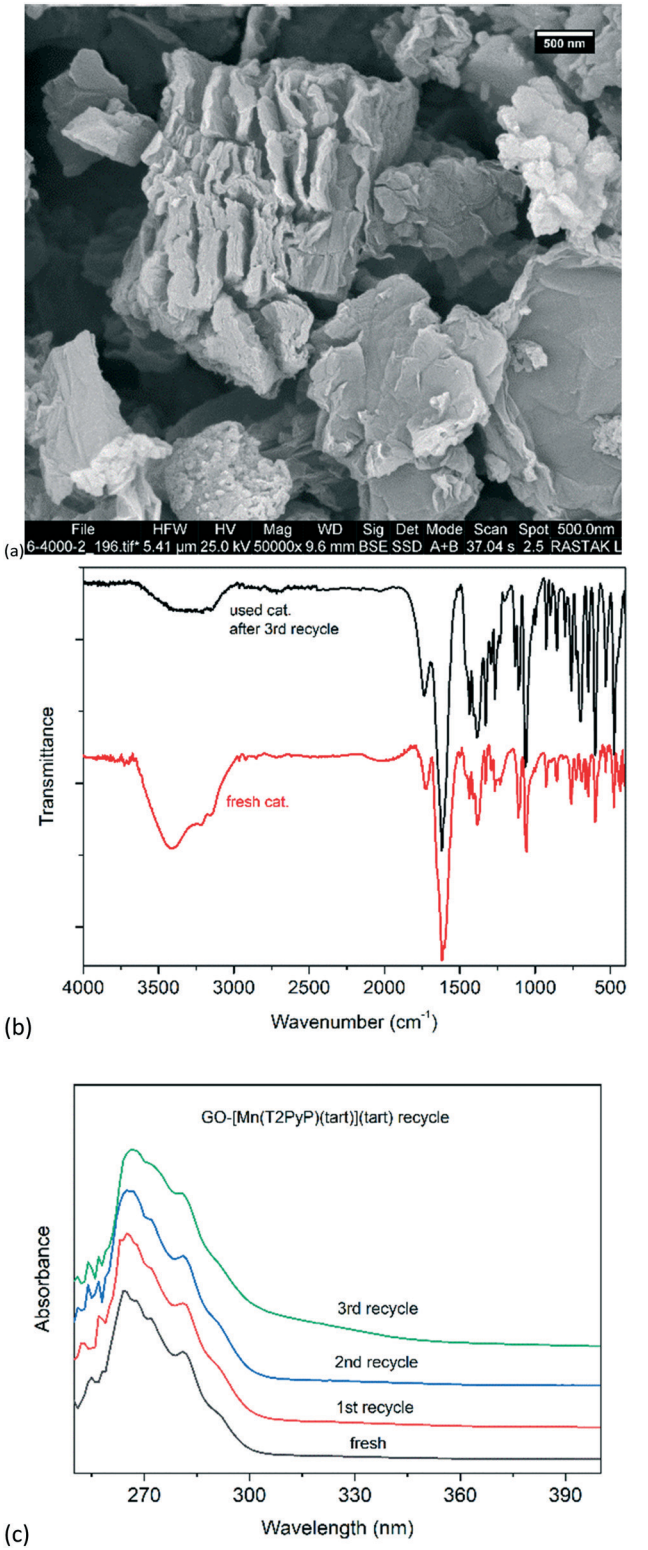

Fig. 9 (a) SEM micrograph and comparison of the (b) FTIR and (c) UV-vis spectra of the fresh and recovered photocatalyst GO-[Mn(T2PyP)(tart)](tart).

In addition to the green nature ($O_2/h\nu$) of the present catalytic system, the enantioselectivity (100% ee), recyclability (100% conversion after three recycles), simplicity and rate in the oxidation are advantages over those of the reported catalysts.[74]

Experimental

Materials and methods

(2*R*,3*R*)-(+)-Tartaric acid, (L-(+)-tartaric acid, Merck, 99%), propionic acid (99%, Merck), (3-chloropropyl)trimethoxysilane (98%, Merck), 2-pyridinecarboxaldehyde (99%, Sigma-Aldrich), manganese(II) acetate (99%, Sigma-Aldrich), hydrogen peroxide (35%, Fluka) were used as received. Pyrrole (97%, Merck) was purified by distillation. Sodium tartrate salt of L-tartaric acid (Na-tart) was prepared as reported already.[48]

For analysis of the reaction products an HP Agilent 6890 gas chromatograph equipped with an HP-5 capillary column (phenyl methyl siloxane 30 m × 320 µm × 0.25 µm) with flame-ionization detector was used. The enantiomeric excess (ee) was determined by an HP 6890-GC using a chiral SGE-CYDEX-B capillary column (25 m × 0.22 mm ID × 0.25 µm). For GC with HP-5 capillary column: injection temperature 250 °C, detector temperature 250 °C, carrier gas N_2 flow rate 0.70 mL min^{-1}; the oven temperature was held at 90 °C for 0.1 min, then heated to 190 °C at a rate of 10 °C min^{-1} and kept for 5 min. For chiral GC with SGE-CYDEX-B capillary column, a column flow of 0.70 mL min^{-1} was applied. The detector and injection temperatures were 200 °C. The oven temperature was held at 50 °C for 0.1 min, then the temperature was increased to 150 °C at a rate of 7 °C min^{-1} and kept for 15 min.

UV-vis spectra of the solutions were run on a Shimadzu 160 spectrometer. Fourier transform infrared (FTIR) spectra were taken using a Perkin-Elmer 597 spectrophotometer. Powder X-ray diffraction patterns were collected at a Bruker D8 ADVANCE, wavelength 1.5406 Å (Cu Kα), voltage 40 kV, current 40 mA. ^{1}H- and ^{13}C-NMR spectra of the reaction mixtures (without purification) were run on a Bruker 250 MHz spectrometer using $CDCl_3$ as solvent. Atom absorption spectroscopy (AAS) was performed by a Varian Spectra 220. Scanning electron microscopy–energy dispersive X–ray spectroscopy (SEM–EDX) were taken using a Hitachi F4160 and a FEI ESEM QUANTA 200. The given gold, copper and zinc content in the EDX spectra and element list is due to the sputtered gold surface of the sample and the brass (Cu/Zn) sample holder. Transmission electron microscopic (TEM) images were generated by a Zeiss 902A electron microscope. Fluorescence spectra were acquired by a CARY ECLIPSE/VARIAN AVANTA 125. The thermal stability of the materials was studied under nitrogen using a STA 504 (BAHR) and a thermogravimetric analyzer (Pyris Diamond).

Synthesis of graphene oxide and its functionalization to GO–Cl. The typical synthesis of graphene oxide (GO) was as follows: a mixture of concentrated sulfuric acid and phosphoric acid (60 : 6 v/v) was prepared and cooled in an ice bath; to this solution graphite powder (2.0 g) and $KMnO_4$ (12.0 g) were added.[75] After stirring for 30 min at room temperature, the mixture was stirred for 24 h at 70 °C. When the mixture was cooled down, 6 mL of hydrogen peroxide

was added. For purification of the resulting GO the product was washed with deionized water, hydrochloric solution, ethanol and diethyl ether. Yield 1.65 g.

As-synthesized GO was functionalized with chloro-propyl units by dispersing 1.0 g of GO in 40 mL dry toluene using an ultrasound bath. 50.0 mmol of (3-chloropropyl)-triethoxysilane was added and the mixture was refluxed under nitrogen atmosphere overnight. The obtained brown solid of GO–Cl was consequently washed with toluene (3 × 7 mL) and ethanol (3 × 7 mL) and dried for 6 h at 60 °C.

Synthesis of 5,10,15,20-tetra(2-pyridyl)porphyrin, H_2TPyP. 2-Pyridylcarboxaldehyde (0.16 mol) and freshly distilled pyrrole (0.16 mol) were dissolved in propionic acid (500 mL) and refluxed for 1 h. At the end of the reaction, distilled water (150 ml) was added to the cooled mixture and the product was extracted using dichloromethane (400 mL). Yield: 3.36 g, 38%.

Synthesis of [Mn(T2PyP)(OAc)]. Following the method of Zakavi *et al.*,[76] a mixture of H2TPyP (3.2 g, 5.17 mmol) and manganese(II) acetate dihydrate (12.6 g, 51.6 mmol) in 400 mL of glacial acetic acid was refluxed at 80 °C for 6 h. The solvent was removed under vacuum and the solid residue dissolved in water (2000 mL) at 60 °C. The mixture was filtered and the metalloporphyrin was precipitated by the addition of sodium acetate solution (300 mL, 2 mol L^{-1}). Yield: 0.245 g, 77%.

Covalent grafting of [Mn(T2PyP)(OAc)] on GO–Cl. GO–Cl (1.20 g) was dispersed in DMF (200 mL) and after addition of [Mn(T2PyP)]OAc (0.120 g, 0.164 mmol), the suspension heated at 100 °C for 48 h under vigorous stirring. The obtained black solid of GO-[Mn(T2PyP)(OAc)]Cl was isolated by centrifugation, washed several times with methanol and diethyl ether. After that, the solid was dried at 60 °C for 6 h.

Synthesis of GO-[Mn(T2PyP)(tart)](tart). The chloride counter ion of GO-[Mn(T2PyP)Cl]OAc was replaced with a tartrate anion. Sodium tartrate (150 mg, 0.618 mmol) was dissolved in 40 mL of methanol and after addition of GO-[Mn(T2PyP)Cl]OAc (100 mg) to the solution, it was stirred for 5 h at 40 °C. The synthesized GO-[Mn(T2PyP)(tart)](tart) was washed with methanol and then fully dried at 60 °C in an oven. An atomic absorption spectroscopic determination yielded 17.87 μmol manganese per gram of GO-[Mn(T2PyP)(tart)](tart), corresponding to 0.098 wt% Mn.

Photocatalytic epoxidation of stilbene by molecular oxygen. The solution of [Mn(T2PyP)(OAc)] (0.50 mg, 0.71 μmol) or dispersion of GO-[Mn(T2PyP)(tart)](tart) (0.0397 g, 0.71 μmol) and imidazole (1.42 μmol) in 1 mL of CH_2Cl_2 was stirred in a thermostatic bath at 25 °C for 1 h. To this dispersion, *trans*-stilbene (0.71 mmol) and isobutyraldehyde (3.55 mmol) as oxygen acceptor (3.55 mmol, 5 equiv. with respect to *trans*-stilbene) were added and after applying oxygen gas through a balloon, the reaction was irradiated by a white LED light (40 W) at room temperature in a black box for the required time. The reaction was followed in time by thin-layer chromatography every 15 min. During the reaction, aliquots of the reaction mixture (2 μL) were withdrawn and analyzed by GC at the same time. Authentic samples and spectroscopic methods (^{1}H-NMR and ^{13}C-NMR) were also used for the identification of the products.

Conclusions

In summary, we have developed a new photocatalytic and asymmetric system that could catalyze the epoxidation of *trans*-stilbene with molecular oxygen with remarkable enantioselectivity and activity. Addition of imidazole as axial ligand improved the photocatalyst activity and its presence was necessary for asymmetric epoxidation. Imidazole gave the best enhancement on the rate of oxygen atom transfer from the suggested reactive intermediate [Mn═O] to the substrate among the investigated nitrogen donor ligands. Furthermore, GO-[Mn(T2PyP)(tart)](tart) could be recovered easily and reused in the asymmetric oxidation of the *trans*-stilbene precursor for at least three times without any considerable loss of its catalytic activity and selectivity. Considering the non-toxic nature of Mn(III) ions and visible white LED light, GO-[Mn(T2PyP)(tart)](tart) is expected to have potential applications in the green synthesis of chiral epoxides using sun light.

Conflicts of interest

There are no conflicts to declare.

Acknowledgements

The authors gratefully acknowledge the financial support from the University of Zanjan and Amirkabir University of Technology.

Notes and references

1 S. C. Stinson, *Chem. Eng. News*, 2000, **78**, 55.
2 J. Larrow and E. Jacobsen, *Chem*, 2004, **6**, 123.
3 R. L. Davis, J. Stiller, T. Naicker, H. Jiang and K. A. Jørgensen, *Angew. Chem., Int. Ed.*, 2014, **53**, 7406–7426.
4 L. Hadian-Dehkordi and H. Hosseini-Monfared, *Green Chem.*, 2016, **18**, 497–507.
5 N. Ananthi and I. M. V. Enoch, *Chirality*, 2019, **31**, 155–163.
6 A. Farokhi, K. Berijani and H. Hosseini-Monfared, *Catal. Lett.*, 2018, **148**, 2608–2618.
7 W. Yan, J. Wang, J. Ding, P. Sun, S. Zhang, J. Shen and X. Jin, *Dalton Trans.*, 2019, **48**, 16827–16843.
8 X. Song, W. Zhu, Y. Yan, H. Gao, W. Gao, W. Zhang and M. Jia, *J. Mol. Catal. A: Chem.*, 2016, **413**, 32–39.
9 P. G. Falkowski and J. A. Raven, *Aquatic photosynthesis*, Princeton University Press, 2013.
10 J.-M. Herrmann, C. Guillard and P. Pichat, *Catal. Today*, 1993, **17**, 7–20.
11 D. E. Dolmans, D. Fukumura and R. K. Jain, *Nat. Rev. Cancer*, 2003, **3**, 380–387.
12 X. Zhou, F. Li, X. Li, H. Li, Y. Wang and L. Sun, *Dalton Trans.*, 2015, **44**, 475–479.

13 E. S. Da Silva, N. M. Moura, M. G. P. Neves, A. Coutinho, M. Prieto, C. G. Silva and J. L. Faria, *Appl. Catal., B*, 2018, **221**, 56–69.
14 G. Bian, P. Jiang, F. Wang, Y. Shen, K. Jiang, L. Liu and W. Zhang, *New J. Chem.*, 2018, **42**, 85–90.
15 R. Ge, X. Li, S.-Z. Kang, L. Qin and G. Li, *Appl. Catal., B*, 2016, **187**, 67–74.
16 M. Neamțu, C. Nădejde, V.-D. Hodoroaba, R. J. Schneider and U. Panne, *Appl. Catal., B*, 2018, **232**, 553–561.
17 M. Hajimohammadi, N. Safari, H. Mofakham and A. Shaabani, *Tetrahedron Lett.*, 2010, **51**, 4061–4065.
18 S. S. Mehrabi-Kalajahi, M. Hajimohammadi and N. Safari, *J. Iran. Chem. Soc.*, 2016, **13**, 1069–1076.
19 S. S. M. Kalajahi, M. Hajimohammadi and N. Safari, *React. Kinet., Mech. Catal.*, 2014, **113**, 629–640.
20 C. M. Neves, O. M. Filipe, N. Mota, S. A. Santos, A. J. Silvestre, E. B. Santos, M. G. P. Neves and M. M. Simões, *J. Hazard. Mater.*, 2019, **370**, 13–23.
21 A. G. Mojarrad and S. Zakavi, *RSC Adv.*, 2016, **6**, 100931–100938.
22 M. Hajimohammadi, F. Bahadoran, S. S. H. Davarani and N. Safari, *React. Kinet., Mech. Catal.*, 2010, **99**, 243–250.
23 T. Montagnon, M. Tofi and G. Vassilikogiannakis, *Acc. Chem. Res.*, 2008, **41**, 1001–1011.
24 H. Hennig, *Coord. Chem. Rev.*, 1999, **182**, 101–123.
25 M. de Torres, R. van Hameren, R. J. Nolte, A. E. Rowan and J. A. Elemans, *Chem. Commun.*, 2013, **49**, 10787–10789.
26 D. Shen, C. Saracini, Y.-M. Lee, W. Sun, S. Fukuzumi and W. Nam, *J. Am. Chem. Soc.*, 2016, **138**, 15857–15860.
27 V. Georgakilas, M. Otyepka, A. B. Bourlinos, V. Chandra, N. Kim, K. C. Kemp, P. Hobza, R. Zboril and K. S. Kim, *Chem. Rev.*, 2012, **112**, 6156–6214.
28 A. D. Adler, *J. Inorg. Nucl. Chem.*, 1970, **32**, 2443–2445.
29 A. Harriman and G. Porter, *J. Chem. Soc., Faraday Trans. 2*, 1979, **75**, 1532–1542.
30 J. J. Li, *Name reactions in heterocyclic chemistry*, John Wiley & Sons, 2004.
31 Y. Xu, H. Bai, G. Lu, C. Li and G. Shi, *J. Am. Chem. Soc.*, 2008, **130**, 5856–5857.
32 Y. Gao, Y. Zhang, C. Qiu and J. Zhao, *Appl. Organomet. Chem.*, 2011, **25**, 54–60.
33 P. Bhanja, S. K. Das, A. K. Patra and A. Bhaumik, *RSC Adv.*, 2016, **6**, 72055–72068.
34 B. Zahed and H. Hosseini-Monfared, *Appl. Surf. Sci.*, 2015, **328**, 536–547.
35 J. Karolczak, D. Kowalska, A. Lukaszewicz, A. Maciejewski and R. P. Steer, *J. Phys. Chem. A*, 2004, **108**, 4570–4575.
36 A. Ogunsipe, J.-Y. Chen and T. Nyokong, *New J. Chem.*, 2004, **28**, 822–827.
37 S. Stankovich, R. D. Piner, S. T. Nguyen and R. S. Ruoff, *Carbon*, 2006, **44**, 3342–3347.
38 B. Ramezanzadeh, Z. Haeri and M. Ramezanzadeh, *Chem. Eng. J.*, 2016, **303**, 511–528.
39 D. Chen, K. Wang, W. Hong, R. Zong, W. Yao and Y. Zhu, *Appl. Catal., B*, 2015, **166**, 366–373.
40 L. Vanoye, Z. E. Hamami, J. Wang, C. de Bellefon, P. Fongarland and A. Favre-Réguillon, *Eur. J. Lipid Sci. Technol.*, 2017, **119**, 1600281.
41 P. Battioni, J. Renaud, J. Bartoli, M. Reina-Artiles, M. Fort and D. Mansuy, *J. Am. Chem. Soc.*, 1988, **110**, 8462–8470.
42 T.-S. Lai, S. K. Lee, L.-L. Yeung, H.-Y. Liu, I. D. Williams and C. K. Chang, *Chem. Commun.*, 2003, 620–621.
43 A. W. Van Der Made and R. J. Nolte, *J. Mol. Catal.*, 1984, **26**, 333–335.
44 H.-Y. Liu, H. Zhou, L.-Y. Liu, X. Ying, H.-F. Jiang and C.-K. Chang, *Chem. Lett.*, 2007, **36**, 274–275.
45 T.-S. Lai, K.-H. Ng, H.-Y. Liu, C. K. Chang and L.-L. Yeung, *Synlett*, 2002, **2002**, 1475–1478.
46 K. Jørgensen and P. Swanstrøm, *Acta Chem. Scand.*, 1988, **43**, 822–824.
47 E. Ahadi, H. Hosseini-Monfared, C. Schlüsener, C. Janiak and A. Farokhi, *Catal. Lett.*, 2020, **150**, 861–873.
48 K. Berijani, A. Farokhi, H. Hosseini-Monfared and C. Janiak, *Tetrahedron*, 2018, **74**, 2202–2210.
49 K. Berijani and H. Hosseini-Monfared, *Inorg. Chim. Acta*, 2018, **471**, 113–120.
50 A. Farokhi and H. H. Monfared, *J. Catal.*, 2017, **352**, 229–238.
51 R. Lechner, S. Kümmel and B. König, *Photochem. Photobiol. Sci.*, 2010, **9**, 1367–1377.
52 D. Mohajer, G. Karimipour and M. Bagherzadeh, *New J. Chem.*, 2004, **28**, 740–747.
53 Y. Li, J.-S. Huang, Z.-Y. Zhou, C.-M. Che and X.-Z. You, *J. Am. Chem. Soc.*, 2002, **124**, 13185–13193.
54 K. Auclair, P. Moënne-Loccoz and P. R. Ortiz de Montellano, *J. Am. Chem. Soc.*, 2001, **123**, 4877–4885.
55 S. Q. Liu, J. Pécaut and J. C. Marchon, *Eur. J. Inorg. Chem.*, 2002, **2002**, 1823–1826.
56 J. A. Elemans, E. J. Bijsterveld, A. E. Rowan and R. J. Nolte, *Chem. Commun.*, 2000, 2443–2444.
57 J. Haber, M. Kłosowski and J. Połtowicz, *J. Mol. Catal. A: Chem.*, 2003, **201**, 167–178.
58 W. Nam, S. J. Baek, K. A. Lee, B. T. Ahn, J. G. Muller, C. J. Burrows and J. S. Valentine, *Inorg. Chem.*, 1996, **35**, 6632–6633.
59 X. Zhou and H. Ji, *Chem. Eng. J.*, 2010, **156**, 411–417.
60 J. Rosenthal, T. D. Luckett, J. M. Hodgkiss and D. G. Nocera, *J. Am. Chem. Soc.*, 2006, **128**, 6546–6547.
61 H. Hennig, J. Behling, R. Meusinger and L. Weber, *Chem. Ber.*, 1995, **128**, 229–234.
62 J. Jung, K. Ohkubo, D. P. Goldberg and S. Fukuzumi, *J. Phys. Chem. A*, 2014, **118**, 6223–6229.
63 L. Weber, J. Behling, G. Haufe and H. Hennig, *J. Prakt. Chem./Chem.-Ztg.*, 1992, **334**, 265–268.
64 K. A. Prokop and D. P. Goldberg, *J. Am. Chem. Soc.*, 2012, **134**, 8014–8017.
65 K. Ishii, *Coord. Chem. Rev.*, 2012, **256**, 1556–1568.
66 R. Bonnett, *Chem. Soc. Rev.*, 1995, **24**, 19–33.
67 A. Farokhi and H. Hosseini-Monfared, *New J. Chem.*, 2016, **40**, 5032–5043.
68 K. E. Simmons and D. E. Van Sickle, *J. Am. Chem. Soc.*, 1973, **95**, 7759–7763.
69 M. J. Gunter and P. Turner, *J. Mol. Catal.*, 1991, **66**, 121–141.

70 T. G. Traylor, *Pure Appl. Chem.*, 1991, **63**, 265–274.
71 G. Tondreau and D. Sweigart, *Inorg. Chem.*, 1984, **23**, 1060–1065.
72 S. Zakavi, A. Abasi, A. R. Pourali and S. Talebzadeh, *Bull. Korean Chem. Soc.*, 2012, **33**, 35–38.
73 R. A. Baglia, C. M. Krest, T. Yang, P. Leeladee and D. P. Goldberg, *Inorg. Chem.*, 2016, **55**, 10800–10809.
74 I. Bernar, F. P. Rutjes, J. A. Elemans and R. J. Nolte, *Catalysts*, 2019, **9**, 195.
75 D. C. Marcano, D. V. Kosynkin, J. M. Berlin, A. Sinitskii, Z. Sun, A. Slesarev, L. B. Alemany, W. Lu and J. M. Tour, *ACS Nano*, 2010, **4**, 4806–4814.
76 S. Zakavi, A. G. Mojarrad and T. M. Yazdely, *Makrogeterotsikly*, 2012, **5**, 67–71.

